Scanning gate microscopy on graphene: charge inhomogeneity and extrinsic doping

2011 Nanotechnology 22 295705

(http://iopscience.iop.org/0957-4484/22/29/295705)

Nanotechnology **22** (2011) 295705 (9pp) doi:10.1088/0957-4484/22/29/295705

Scanning gate microscopy on graphene: charge inhomogeneity and extrinsic doping

Romaneh Jalilian[1,2,7], Luis A Jauregui[2,3], Gabriel Lopez[2,3,8], Jifa Tian[1,2], Caleb Roecker[4], Mehdi M Yazdanpanah[5,6], Robert W Cohn[6], Igor Jovanovic[4,9] and Yong P Chen[1,2,3]

[1] Department of Physics, Purdue University, West Lafayette, IN 47907, USA
[2] Birck Nanotechnology Center, Purdue University, West Lafayette, IN 47907, USA
[3] School of Electrical and Computer Engineering, Purdue University, West Lafayette, IN 47907, USA
[4] School of Nuclear Engineering, Purdue University, West Lafayette, IN 47907, USA
[5] NaugaNeedles LLC, Louisville, KY 40299, USA
[6] Department of Electrical Engineering, University of Louisville, Louisville, KY 40292, USA

E-mail: yongchen@purdue.edu

Received 11 March 2011, in final form 2 May 2011
Published 16 June 2011
Online at stacks.iop.org/Nano/22/295705

Abstract
We have performed scanning gate microscopy (SGM) on graphene field effect transistors (GFET) using a biased metallic nanowire coated with a dielectric layer as a contact mode tip and local top gate. Electrical transport through graphene at various back gate voltages is monitored as a function of tip voltage and tip position. Near the Dirac point, the response of graphene resistance to the tip voltage shows significant variation with tip position, and SGM imaging displays mesoscopic domains of electron-doped and hole-doped regions. Our measurements reveal substantial spatial fluctuation in the carrier density in graphene due to extrinsic local doping from sources such as metal contacts, graphene edges, structural defects and resist residues. Our scanning gate measurements also demonstrate graphene's excellent capability to sense the local electric field and charges.

(Some figures in this article are in colour only in the electronic version)

1. Introduction

The past few years have witnessed intensive research on graphene (2D carbon), a single layer graphite with unique electronic properties [1–3] and exciting promise for applications ranging from nanoelectronics to sensors. As a zero-gap semiconductor (semimetal), graphene's conduction and valence bands touch at the charge-neutral Dirac point (DP) with relativistic linear energy–momentum dispersion [1]. Intrinsically charge-neutral, graphene can be easily doped electrically or chemically [3–6]. For example, in a typical graphene field effect transistor (GFET), a voltage applied to a gate (capacitively coupled to graphene) can tune the charge carriers (effectively tuning the Fermi energy relative to the DP) from p-type (holes) to n-type (electrons), with the graphene resistance peaking at the charge-neutral DP [1, 3]. Such an ambipolar electric field effect, which can exhibit high mobility even at room temperature, underlies the operation of most graphene devices. The finite minimum conductivity (which varies from sample to sample and shows discrepancies with earlier theories [1]) experimentally observed in graphene at the DP has been a subject of much discussion. It is now realized that the values of minimum conductivity measured in realistic samples can be largely related to charge inhomogeneity [7, 8] in graphene, where the local charge density remains finite in the form of electron and hole puddles even at zero

[7] Present address: NaugaNeedles LLC, Louisville, KY 40299, USA.
[8] Present address: Sandia National Laboratories, Livermore, CA 94550, USA.
[9] Present address: Department of Mechanical and Nuclear Engineering, The Pennsylvania State University, State College, PA 16802, USA.

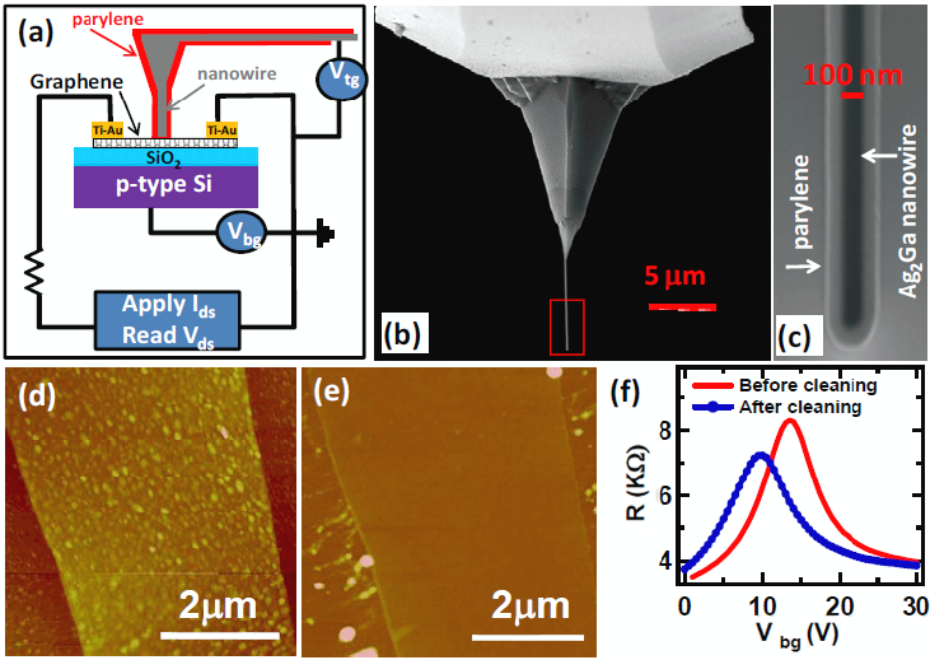

Figure 1. (a) Schematic of the experimental set up for contact mode scanning gate microscopy (SGM) on graphene. (b) SEM image of a custom-made contact mode SGM tip. (c) Magnified view of the end of the tip, showing a conductive Ag_2Ga nanowire surrounded by parylene (dielectric) coating. (d) AFM image (tapping mode) of a graphene covered by residues from the device fabrication process. (e) Image of the same device in (d) after 'nano-broom' cleaning by contact mode AFM. (f) The field effect (resistance versus back gate voltage) of the GFET device before (d) and after (e) AFM cleaning.

average charge carrier density at the (global) charge-neutral DP. Various sources, such as topographic corrugations (e.g. ripples of graphene) [9], charged impurities [10, 11], adsorbed molecules [5], surface contaminants [12] and metal contacts [6, 13] have been suggested that could cause local doping and thus inhomogeneous charge density in graphene. The length scales of the resulting charge puddles and doping domains can range from nanometers (e.g. in the case of charged impurities [11]) to microns (e.g. in the case of metal contact [13]).

While transport experiments can explore the signatures of inhomogeneous charge density and doping in graphene [14–16], scanning probe microscopy (SPM) measurements provide the most direct probe of local electronic properties. Martin *et al* demonstrated the formation of sub-micron (resolution limited) electron and hole charge puddles near the DP in graphene using scanning single-electron transistor (SET) microscopy, and inferred the intrinsic size of the puddles to be ∼30 nm from measurements in the quantum Hall regime [8]. High-resolution scanning tunneling microscopy (STM) experiments have directly imaged charge puddles of ∼10 nm in size, with the suggestion that they originate from individual charged impurities underneath graphene [11, 17]. Scanning photocurrent microscopy (SPCM) revealed modulations in the electrical potential across the graphene (particularly near electrodes) and gave evidence for metal-induced doping [18, 19], although alternative interpretations of SPCM data in terms of photothermal electric effects (PTE) have also been suggested [20].

In this paper, we report our study using atomic force microscope (AFM) based scanning gate microscopy (SGM) to probe the local electronic properties and charge inhomogeneity in graphene (exfoliated and supported on SiO_2). In SGM [21–29], a charged tip is used as a movable local top gate to modulate the carrier density underneath the tip in a device whose resistance (or conductance) is measured. Scanning the tip (top gate) over the device generates a map showing how the electrical resistance (or conductance) through the device depends on the tip-induced local density modulation (local potential) at various locations. SGM has been previously applied to study the local electronic properties and defects in semiconductor nanostructures [21–24], nanowires [25] and carbon nanotubes (CNT) [26–29]. Similar techniques have recently been applied to graphene for studying the effects of local scattering potential on the quantum interference of carriers [30], imaging localized states in graphene nanostructures [31], studying effects of current annealing on electronic uniformity [32], and performing various other analyses of graphene layers [33]. Previous SGM measurements were typically performed in the 'lift mode', where a biased conductive AFM tip is kept at a constant height (with possibly a small modulation [34]) above the device surface and the corresponding sample conductance response is measured. Sensitivity, spatial resolution (nonlocal effects of the tip), measurement synchronization, tip drift over time and potential tip–sample shortage (due to electrostatic attraction) are some of the common challenges [22, 34]. In our work, we used an alternative method to perform SGM based on contact mode AFM with a dielectric-coated metallic nanowire as the tip (figures 1(a)–(c)). This scheme simplifies the SGM measurements with a number of technical

advantages to be discussed below. Employing such a contact mode SGM, we have obtained clear images demonstrating electronic inhomogeneity in graphene, particularly charge puddles formed near the DP. Our results provide evidence for the local and extrinsic doping induced by metal contacts and graphene edges as important sources of charge density inhomogeneity and puddles of size reaching few microns. We also demonstrate surface contamination as another source of extrinsic doping, and clean such contamination with an AFM tip. Our findings, together with (and complementing) those from earlier SPM measurements (e.g. STM, which has higher spatial resolution while probing a smaller area of sample than ours), show that charge inhomogeneity in realistic graphene samples can occur at multiple length scales (ranging from nanometers to microns) owing to a multitude of extrinsic doping sources. Meanwhile, our scanning gate measurements also demonstrate graphene's excellent capability to sense (through its resistance change) the presence of a local electric field and/or charges.

2. Experimental details

The experimental setup of our contact mode SGM is schematically shown in figure 1(a). One electrode ('drain') of the graphene device was grounded and DC bias voltages were applied to the tip (local top gate) and/or substrate (back gate). The graphene resistance (R) was measured at room temperature (300 K) and by passing a small DC source–drain current ($I_{ds} = 1\ \mu$A) while measuring the voltage drop (V_{ds}) across the sample. We believe our measurements were in the 'Ohmic' regime, because further reducing the current did not give an appreciable difference in the results. We have performed two-terminal, three-terminal and four-terminal measurements on various devices yielding qualitatively similar results for the purpose of this work. V_{ds} can be fed into the AFM controller while scanning the tip to produce SGM images. Each SGM image has 512 lines and each line (scanned at a rate of 0.68 Hz) contains 512 sample points.

Contact mode AFM cantilever probes (spring constant 0.1 N m^{-1}) with metallic Ag_2Ga nanowires (NWs) of high aspect ratio (50:1) at the end (HARNP-C20, NaugaNeedles, KY, USA) were used for this study (figures 1(b) and (c)). The flexible tip has a gentler contact with the surface that prevents scratching of the graphene. The high aspect ratio and cylindrical structure of the NW reduce the parasitic capacitance between the tip (top gate) and the sample. The Ag_2Ga NW is grown by immersion of the AFM tip (coated with a silver film, thickness 50–100 nm) in a small Ga droplet followed by slow extraction of the cantilever from the droplet [35, 36]. The NWs used in this work have a typical diameter in the range of 50–100 nm and length of 1–5 μm. For the top gate dielectric, we used parylene-N (typical thickness in the range of 50–100 nm, deposited in a thermal chemical vapor deposition system) conformally coated on the AFM tip with the NW (figure 1(c)). The uniform parylene coating facilitates a well-controlled dielectric thickness for the contact mode scanning top gate that prevents electrical leakage (tip–graphene shortage) and is also less susceptible to tip drift than conventional lift mode SGM.

The monolayer graphene samples used in our experiments were fabricated by mechanical exfoliation [3]of highly ordered pyrolytic graphite (HOPG) on 300 nm (thermally grown) SiO_2 on p-type doped Si substrate (back gate). The samples are fabricated into GFET devices using e-beam lithography with evaporated Ti–Au (5–45 nm) contact electrodes. Monolayer graphene is selected by optical microscopy and confirmed by Raman spectroscopy [37], and further verified by quantum Hall measurements [38, 39] in selected devices. The mobility of our typical GFET devices is measured to be $\sim$3000 cm^2 V^{-1} s^{-1}.

Standard back-gated field effect measurements typically show a positive DP in our graphene devices (figure 1(f)), indicating extrinsic hole doping. Common sources for such doping include moisture from the ambient environment and residues (e.g. PMMA resist) from device fabrication processes. We have used regular contact mode AFM to sweep away the dusts and residues on the graphene surface and found that such AFM cleaning can reduce the extrinsic hole doping (down-shift the DP voltage), as demonstrated in figures 1(d)–(f) for a device with a particularly high degree of residue coverage. Such cleaning is routinely performed for a more stable device response in subsequent contact mode SGM. Topography of the graphene can be measured simultaneously during the contact mode SGM, although regular tapping mode AFM is also performed to obtain topographic images of slightly better quality.

3. Results

The main results of this paper (scanning gate measurements) are presented in figures 2–4. Multiple devices have been studied with qualitatively similar findings and representative data from three devices ('A', 'B' and 'C') will be presented below. We first show the effect of local top gate (AFM tip) voltage on graphene resistance. The AFM image (tapping mode) of the device (sample A) used for this measurement is shown in figure 2(a). Figure 2(b) shows the 'global' field effect by sweeping the back gate voltage (V_{bg}), which controls the global average charge carrier density ($\langle n \rangle$) in graphene. The global DP voltage (V_{DP}) is 8.5 V for this device. Figures 2(c)–(e) show R measured as a function of top gate voltage (V_{tg}, swept from -20 to 20 V) applied to the AFM tip for two different tip locations (marked in figure 2(a) as L1 and L2) and at fixed back gate voltages of (c) $V_{bg} = 0$ V, (d) $V_{bg} = 8.5$ V and (e) $V_{bg} = 20$ V, respectively. In figure 2(c) ($V_{bg} < V_{DP}$), the graphene is heavily p-type (with $\langle n \rangle \sim +6 \times 10^{11}$ cm^{-2}, estimated from the global field effect[10] shown in figure 2(b)) and R increases with increasing V_{tg} (within the range measured) for both tip locations. The opposite behavior is seen in figure 2(e) ($V_{bg} > V_{DP}$), where the graphene is heavily n-type ($\langle n \rangle \sim -8 \times 10^{11}$ cm^{-2}) and R decreases with increasing V_{tg} (within the measurement range). In figure 2(d) ($V_{bg} = V_{DP}$), where the graphene is at its global charge-neutral DP ($\langle n \rangle \sim 0$), the R–V_{tg} curve is generally non-monotonic within the range of measurement and displays a peak, which we call the 'local' Dirac point (LDP). Furthermore, the R–V_{tg}

[10] We have $\langle n \rangle = C(V_{DP} - V_{bg})$, where $C = 1.15 \times 10^{-4}$ C V^{-1} m^{-2} is the capacitance per unit area between the graphene and the back gate.

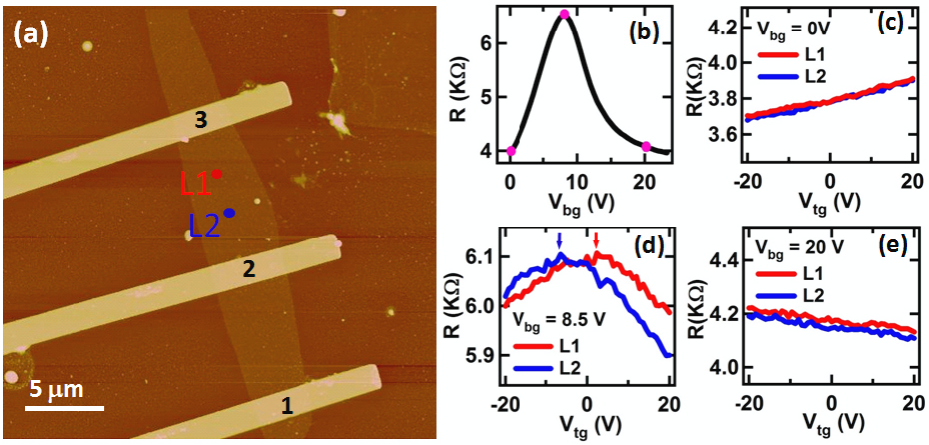

Figure 2. Global and local field effect (sample 'A'). (a) AFM image (tapping mode) of the device. The graphene resistance (R) is measured from contact electrode '2' to '3' (with current I_{ds} applied from source '1' to drain '3'). (b) The 'global' field effect: R as a function of global back gate voltage (V_{bg}). The 'global' Dirac point (DP) occurs at $V_{DP} \sim 8.5$ V. (c)–(e) Local field effect: R as a function of local top gate voltage (V_{tg}, applied to the SGM tip) measured at three different back gate voltages: (c) 0 V ($V_{bg} < V_{DP}$), (d) 8.5 V ($V_{bg} = V_{DP}$) and (e) 20 V ($V_{bg} > V_{DP}$). Data measured at two different tip locations (L1 and L2, marked in (a)) are shown in each panel ((c)–(e)). The thickness of the parylene coating used on the AFM tip is 100 nm.

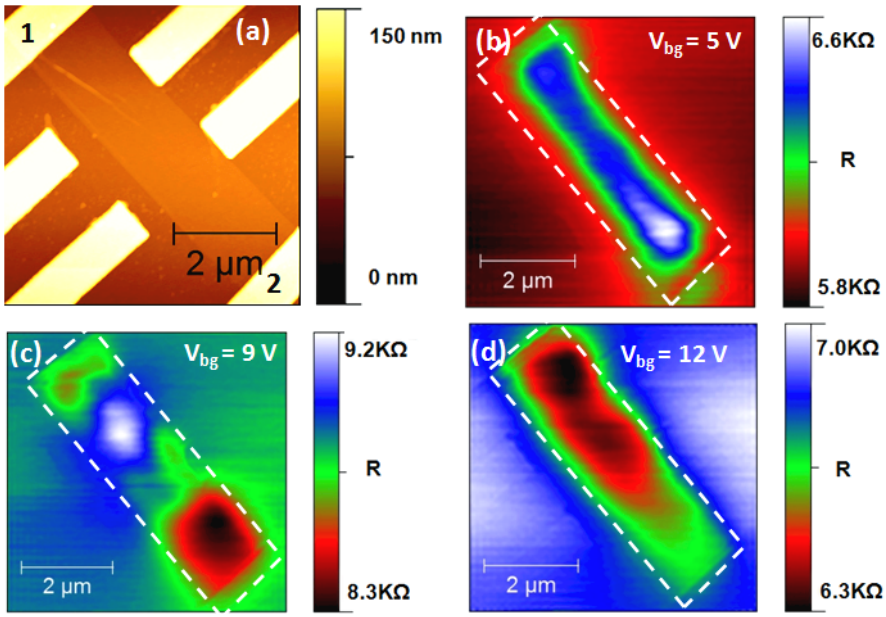

Figure 3. SGM at different back gate voltages (sample 'B'). (a) AFM image (tapping mode) of the device. The graphene resistance (R) was measured from the contact electrode 1 to 2 (with current I_{ds} from 1 to 2, while the other electrodes shown are for a different experiment and are kept floating in the SGM measurement). (b)–(d) SGM image of the GFET measured at three different back gate voltages: (b) 5 V ($V_{bg} < V_{DP}$), (c) 9 V ($V_{bg} = V_{DP}$), and (d) 12 V ($V_{bg} > V_{DP}$). SGM imaging in ((b)–(d)) was performed at a fixed tip voltage ($V_{tg} = 20$ V) and over the same sample area shown in (a). The thickness of the parylene coating on the tip used is 100 nm. In (c) the red puddles (more prominent for the lower contact) near both contact electrodes indicate electron doping, and the blue puddle in the middle of the graphene flake indicates hole doping (see text for more details). White dashed lines in ((b)–(d)) indicate the graphene flake between the two contact electrodes.

dependence is found to be highly dependent on the tip location. For example, for location L1, the LDP occurs at $V_{tg} \sim +3$ V, while for location L2 the LDP occurs for $V_{tg} \sim -6$ V. Such spatial variation of LDP is a result of charge inhomogeneity in the graphene sample, as will be further addressed in the following. As a consistency check to confirm the gating effect of the biased tip, we have retracted the tip far from the graphene surface and observed R becoming insensitive to the voltage and position of the tip.

Figure 3 presents the results of SGM imaging on a GFET (sample 'B', with a global $V_{DP} \sim 9$ V) measured at a constant V_{tg} (20 V) at various V_{bg}. The AFM tapping mode image of this device is shown in figure 3(a). The parylene coating on the AFM tip has a thickness of 100 nm in this measurement. Figures 3(b)–(d) display the SGM image (resistance of GFET as a function of tip position) for $V_{bg} = 5$ V, 9 V and 12 V respectively. In figure 3(b), where $V_{bg} = 5$ V ($<V_{DP}$), placing the tip on the p-type graphene is seen to increase its

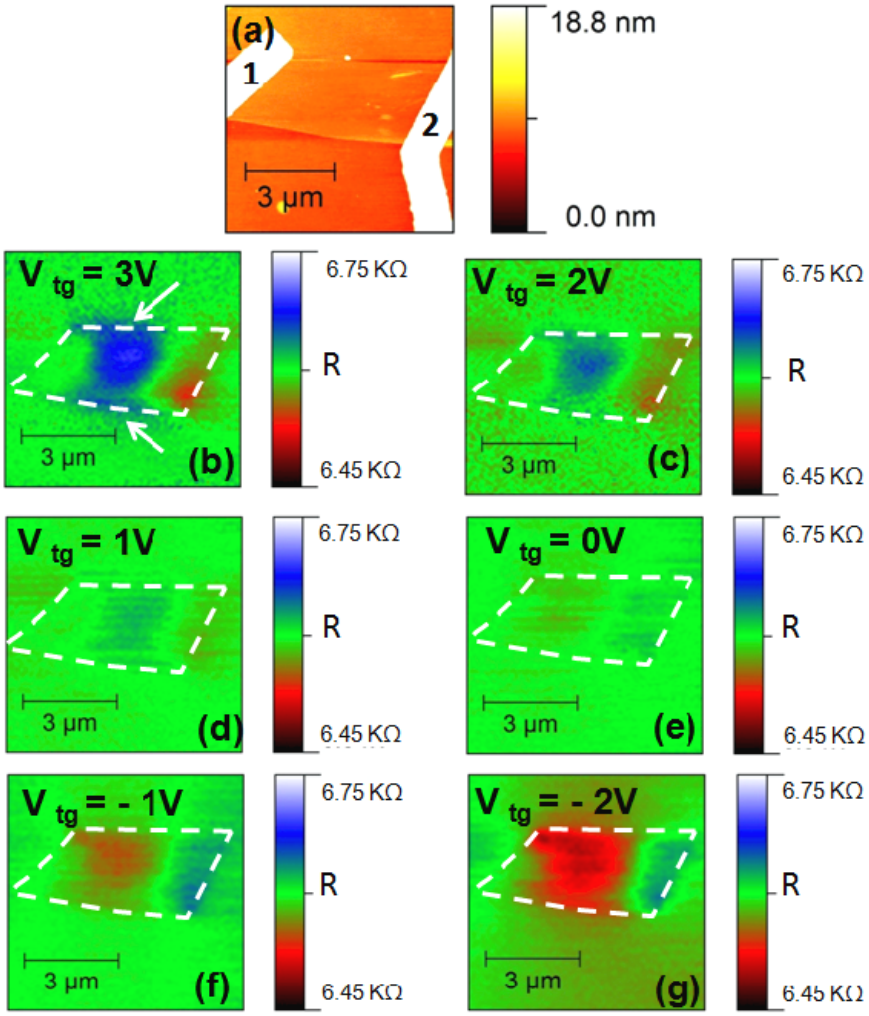

Figure 4. SGM at the global Dirac point (DP) at different top gate voltages (sample 'C'). (a) AFM image (contact mode) of the device. The resistance is measured from contact 1 to 2. (b)–(g) SGM over the same area shown in (a) taken at the DP ($V_{bg} = V_{DP} = 14$ V) with different tip voltages ($V_{tg} = 3, 2, 1, 0, -1, -2$ V, respectively). The same color scale (spanning ∼0.3 kΩ) is used for all SGM images. White dashed lines in (b)–(g) indicate the graphene flake between the electrodes. The white arrows in (b) mark two stripe-shaped 'hole' puddles observed near and parallel to the edges of this graphene sample. The thickness of the parylene coating on the tip used is 50 nm.

resistance R (by as much as nearly 1 kΩ compared to the background value when the tip is far away from graphene), with the graphene appearing blue (indicating higher resistance than the background) in the SGM image. This is due to the local reduction of carrier (hole) density in graphene under the positively biased tip. The opposite behavior is observed in figure 3(d), where $V_{bg} = 12$ V ($> V_{DP}$); placing the tip on the n-type graphene decreases R and makes it appear red (indicating lower resistance than background) in the SGM image. This is due to the local enhancement of carrier (electron) density in graphene under the positively biased tip. However, in figure 3(c), where $V_{bg} = 9$ V (close to V_{DP}) and the graphene is in its global 'charge-neutral' ($\langle n \rangle \sim 0$) state, the 'polarity' of the resistance response of graphene to the tip becomes spatially non-uniform (R can be either increased or decreased depending on the locations of the tip on graphene). In the SGM image, this is manifested as the graphene appearing to break into several 'islands' with very different colors. These 'islands', irregularly shaped and with length scales ranging from ∼0.5 to 2 μm, will be interpreted as resulting from electron or hole 'charge puddles' formed in the graphene near its global 'charge-neutral' DP due to inhomogeneous extrinsic doping.

We have also studied how the SGM image showing the 'puddles' develops with V_{tg} while fixing $V_{bg} \sim V_{DP}$. The results measured for sample 'C' are presented in figure 4. The contact mode AFM image (acquired simultaneously as the SGM images) of this device is shown in figure 4(a). In this experiment, V_{bg} is fixed at 14 V (measured global V_{DP} for this device). The parylene coating on the SGM tip used has a thickness of 50 nm. Figures 4(b)–(g) displays SGM images taken with V_{tg} varying from 3 to −2 V (in 1 V step), plotted with the same color scale and resistance span (from 6.45 to 6.75 kΩ). The 'puddle' pattern, qualitatively similar to that observed in figure 3(c) and in all other samples we measured near the DP, is again observed in figure 4(b) (with a positive $V_{tg} = 3$ V). The pattern (and the magnitude of the spatial variation of resistance response to the tip location) is

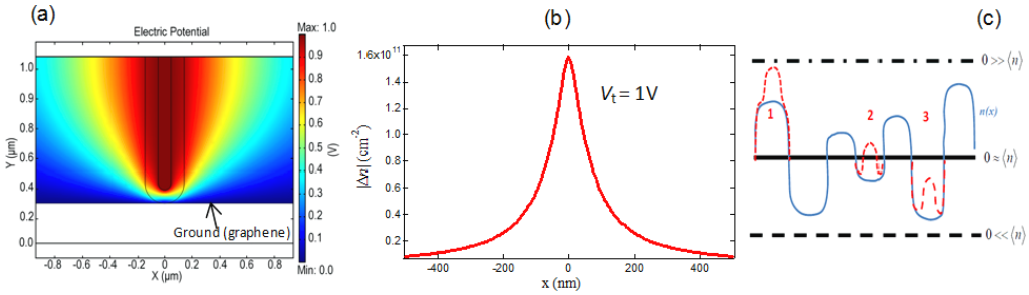

Figure 5. (a) Calculated electric potential of a representative nanowire-based SGM tip (with bias $V_{tg} = 1$ V) in contact with grounded graphene (indicated by an arrow). The thickness of the parylene coating separating the NW and graphene is 100 nm. The geometry is assumed to be radially (x) symmetric and the profile shown is a 2D cross section through the central axis ($x = 0$) of the NW. (b) Calculated profile of charge density induced by the tip as shown in (a). (c) A schematic example of spatially inhomogeneous charge density $n(x)$ (thin blue solid line) and the change (thin red dashed line) due to a negatively biased SGM tip at three representative locations (labeled 1, 2 and 3). The thick black solid line, dot-dashed line and dashed line indicate the zero charge density level for three situations: charge-neutral ($\langle n\rangle \sim 0$, with $V_{bg} \sim V_D$), n-type ($\langle n\rangle \ll 0$, with $V_{bg} > V_D$), and p-type ($\langle n\rangle \gg 0$, with $V_{bg} < V_D$) doping, respectively.

seen to become subdued (figures 4(c)–(e)) as the tip voltage is reduced and almost disappears at $V_{tg} = 0$ V (figure 4(e))[11]. The 'puddle' pattern in the SGM images is seen to reappear for negative V_{tg} (figures 4(f) and (g)), but with reversed 'polarity' (switching the blue and red regions, or enhanced-R or depressed-R regions) in comparison to positive V_{tg}.

4. Discussions

It is known that due to various sources of disorder and extrinsic doping the carrier density in a realistic graphene sample and GFET device is spatially inhomogeneous. A biased SGM tip (top gate) can capacitively induce or deplete charge carriers in graphene. The main features of our observations can be understood simply by considering how the electronic transport of graphene with an inhomogeneous carrier density can be affected by local modulation of charge carriers due to the tip. We have used finite-element analysis (COMSOL) to simulate the electrostatic potential (V) generated by the biased contact mode SGM tip. The result for a representative tip with NW diameter of 100 nm, parylene thickness of 100 nm and V_{tg} of 1 V is shown in figure 5(a). In our model, the tip is assumed to have radial symmetry with a 'round' end (figure 5(a)), a good approximation to the shape shown in the SEM image (figure 1(c)). The graphene is modeled as an electrically grounded plane touching the tip (parylene) at the end point. We have simulated the effect of small variations of the tip geometry and tip–graphene contact area and found that the results do not qualitatively change our conclusions. The biased tip would deplete charge carriers (or induced charges with opposite polarity) in the graphene underneath. The induced surface charge density, calculated from $\frac{\partial V}{\partial y}|_{y\to 0+}$ (change of electric field normal to graphene), for the tip shown in figure 5(a) is plotted (as a function of the radial distance in the graphene plane) in figure 5(b). The locally induced charge density decays away from the tip contact point with a characteristic length scale (full width at half maximum, FWHM) of ∼130 nm. Figure 5(c) schematically depicts a spatially fluctuating carrier density $n(x)$ (thin solid blue line, excluding the tip-induced charges) and how a charged SGM tip may change the carrier density at various locations (thin dashed red line). The picture is drawn for a tip with $V_{tg} < 0$ (the situation is simply reversed for $V_{tg} > 0$). When graphene is globally p-type ($V_{bg} \ll V_{DP}$ and $n(x) \gg 0$, with the thick dashed black line representing the zero carrier density level), a tip with $V_{tg} < 0$ would decrease the graphene resistance (R) by adding charge carriers (holes) to the sample, whereas a tip with moderate[12] $V_{tg} > 0$ would increase R by depleting charge carriers. This is consistent with our observations in figures 2(c) and 3(b). The reverse is true when graphene is n-type ($V_{bg} \gg V_{DP}$ and $n(x) \ll 0$, marked by the thick dot-dashed black line), consistent with our observations in figures 2(e) and 3(d). When graphene is near its (global) 'charge-neutral' state ($V_{bg} \sim V_{DP}$), the average carrier density $\langle n\rangle \sim 0$ (marked by the thick solid black line[13]). Because of the spatial fluctuation in $n(x)$, some regions of the sample have $n(x) > 0$ (hole puddles) and some others have $n(x) < 0$ (electron puddles). Now the response of R would depend on the tip location. As displayed in figure 5(c), a tip with moderate $V_{tg} < 0$ would decrease R when placed above a hole puddle (e.g. location '1') and increase R when placed above an electron puddle (e.g. location '3'), with reversed behavior for a tip with moderate $V_{tg} > 0$. This allows us to identify the 'red-shifted' (lower R) regions in graphene as electron puddles and 'blue-shifted' (higher R) regions as hole puddles in SGM images taken with positively biased tips (e.g. figures 3(c), 4(b) and (c)), and vice versa for SGM images taken with negatively biased tips (figures 4(f) and (g)).

Applying this analysis to figure 2(d), we may associate location L1 with a hole puddle and L2 with an electron puddle from the respective response of R at small V_{tg}. The LDP (maximum R at finite V_{tg}) is understood because a tip that

[11] The small but finite contrast in SGM images even for $V_{tg} = 0$ V may be due to the fringe electric field between the tip and the biased back gate [8], and the work function difference between the tip and graphene [30, 46].

[12] Until $|V_{tg}|$ is sufficiently large so as to induce the opposite-type carriers in graphene and decrease its R. However, excessive $|V_{tg}|$ is typically avoided in our measurements to prevent breakdown of the parylene coating.

[13] Alternatively, one can view the thick black lines as the global chemical potential (Fermi level) set by V_{bg} and the thin line as the locus of DP (local potential) to obtain similar conclusions.

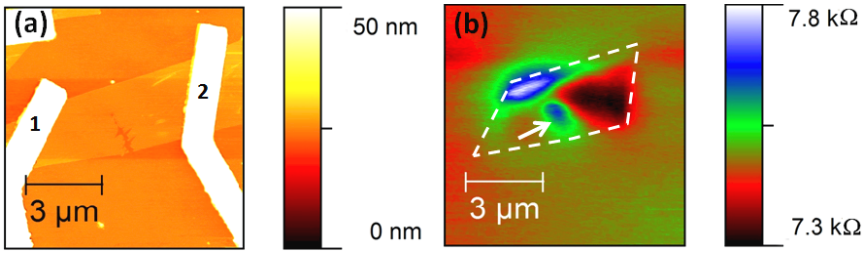

Figure 6. (a) AFM image (contact mode) of sample C (figure 4) after a scratch (indicated by an arrow) was made by the AFM tip. (b) SGM image of the scratched sample biased near its global Dirac point. A hole puddle was observed around the scratch (arrow). $V_{tg} = 5$ V was used in this measurement. Dashed lines in (b) indicate the area of the graphene flake between the electrodes.

depletes local carriers at moderate bias could induce opposite-type carriers (e.g. location '2' depicted in figure 5(c)) in graphene at further increased V_{tg} and eventually lower R when the opposite carriers reach a sufficient number. Therefore, the value of V_{tg} at LDP (together with the calculated tip-induced charge density, figure 5(b)) can be used to give an estimate (which is an upper bound) for the local carrier density $n(x)$: $\sim +5 \times 10^{11}$ cm^{-2} for L1 and $\sim -1 \times 10^{12}$ cm^{-2} for L2. The variation (V_{bg}-independent) of carrier density between the locations, $\sim 1.5 \times 10^{12}$ cm^{-2}, corresponds to a variation of local DP or Fermi energy ($E_F = \hbar v_F \sqrt{\pi n}$) of the order of 100 meV (taking the Fermi velocity [40] in graphene $v_F \sim 1 \times 10^6$ m s^{-1}), similar to the values obtained in other experimental [11, 17] (low T) and theoretical works [41] focusing on length scales smaller than our experiments

The length scale ($\sim$200 nm–2 μm) of the charge puddles we observe in the SGM images taken in our samples at the DP is comparable with the puddle sizes observed in SET [8] and SPC [18, 19] measurements, but much larger than those ($\sim$10–20 nm) observed in STM measurements [11, 17]. This reflects both the diameter ($\sim$100–200 nm) of our tips (similar to those in SPC and SET experiments) and the multiple length scales associated with the charge fluctuations in real graphene samples, as discussed below.

Charge density inhomogeneity (which leads to the formation of electron/hole puddles near the DP) in graphene has been actively studied due to its importance for the electronic properties of graphene and device performance. Various sources have been proposed to cause extrinsic doping resulting in charge inhomogeneity. Such sources include charged impurities near graphene [11, 17], adsorbed molecules [5], surface contaminants (e.g. resist residues) [12], structural disorder in graphene (e.g. ripples [9]) and metal contacts [6, 13]. Our SGM data reveal electron puddles near the contact electrodes in our samples (e.g. figures 3(c) and 4). This is consistent with previous suggestions [6, 18] that Ti (as used in our contacts) could cause n-type doping in graphene. The size of the contact-induced doping regions can reach the micron scale (therefore not tip-resolution-limited), consistent with theoretical predictions [13] and SPCM and SGM measurements [18, 19, 32]. The visibility of the electron puddle can be quite different for different contacts, and may be related to other sources of local and non-uniform doping in the sample. Concomitant with the electron puddles seen near contacts, prominent hole puddles are seen in the middle of the graphene flake (figures 3(c) and 4), keeping the total charge neutrality of the graphene at its DP. Also, we have often observed hole puddles near the edges of graphene (e.g. figure 4(b), indicated by arrows), the extent to which they are observable varying from sample to sample. This suggests that edges, which are chemically more active than the bulk of graphene, tend to hole-dope the graphene, possibly due to the environmental molecules (e.g. H_2O) bonding or adsorbing on the edge. In a different measurement involving sample C, we also observed a hole puddle formed around a scratch made in the graphene (figure 6). The observed width of such edge-induced puddles is comparable with the tip size, and is likely to be resolution limited. Our experiment is relatively insensitive to charge puddles of length scale $<$100 nm, such as those associated with isolated impurities underneath graphene [11]. The puddle pattern is a combined effect of multiple extrinsic doping sources, and generally has substantial variation among different samples. Furthermore, within the resolution of our experiment, we have not detected any correlation between the topography (height fluctuations, measured by regular AFM imaging) of a sample with the 'charge puddle' pattern imaged by SGM near the DP.

While extensively applied to 1D or quasi-1D samples, SGM for 2D conducting thin films is usually challenging [21–29, 34, 42] as the charges added or subtracted (by the SGM tip) from a small fraction of the sample area typically have only very weak effect on the global resistance of the whole sample. The situation for graphene is much better because of the significantly reduced density of states and charge screening [5, 40, 43]. For the SGM tip shown in figures 5(a) and (b), the total number of charges induced/depleted in graphene is calculated to be $\sim 150e$ (for $V_{tg} = 1$ V). From the typical measured top gate local field effect (e.g. figure 2(b)), we estimate that the charge sensitivity of our GFET device (even with its moderate mobility) can reach $\sim$30–50 mΩ/e. This demonstrates the excellent potential of GFETs as room temperature charge sensors.

The transport mean free path l extracted from the carrier mobility is below $\sim$50 nm in our samples, shorter than both the SGM tip size ($\sim$100 nm) and the device size (several microns). Therefore our measurements are performed in the diffusive transport regime. The observation that at the (global) DP, the resistance of graphene can be further increased by the SGM tip bias (e.g. figures 2(d), 3 and 4) demonstrates that the 'minimal conductivity' measured in our graphene device at the DP is not

universal [40], but dependent on the charge inhomogeneity in graphene, as has been pointed out previously [7, 8, 16]. SGM provides a simple way to monitor such a charge inhomogeneity and study its effect on electronic transport in graphene.

As an AFM-based technique, SGM has a number of advantages in probing the local electronic properties of nanoelectronic devices. It can probe and manipulate the local charge or potential profile (e.g. by local gating, or mechanically removing doping sources such as surface residues) and study the influence on the electronic transport through the operating device. SGM can be performed in a wide range of temperature, pressure and various ambient environments, and allows a large area scan. It does not heat the sample as in SPCM [20] and does not have as stringent requirements on substrate conductivity as in STM. Our contact mode technique presented here allows both topographic and SGM images to be simultaneously obtained in one measurement. The high aspect ratio NW tip we employed reduces the parasitic capacitance between the conventional AFM tips with the sample, and has potential benefits for improving spatial resolution. Further technical improvements may include using thinner NWs or carbon nanotubes [44] and thinner dielectric layer on the tips for higher spatial resolution, using tip voltage modulation and lock-in detection to improve the sensitivity, and performing SGM at low temperatures (where the carrier phase coherence length becomes large [45]) to study quantum transport [23, 30, 31] in graphene.

5. Conclusions

In conclusion, realistic graphene devices are subject to various extrinsic sources that locally dope the graphene, resulting in a spatially inhomogeneous charge density and the formation of electron and hole puddles of various length scales at the global charge-neutral Dirac point. We have performed scanning gate microscopy on graphene and observed such charge inhomogeneity and puddles due to extrinsic doping from possible sources such as metal contacts, graphene edges and surface residues. Our measurements were done using contact mode scanning gate microscopy with a tip made of a metallic nanowire coated with a dielectric layer, and it can complement other forms of scanning probe microscopies to reveal the multiple origins of charge inhomogeneity in graphene and how such inhomogeneity can affect the electronic transport of graphene devices. Our scanning gate measurements also demonstrate graphene can be used as an excellent room temperature sensor for local electric field and charges.

Acknowledgments

This work has been partially supported by the National Science Foundation (ECCS#0833689), Department of Homeland Security (#2009-DN-077-ARI036-02), Nanoelectronic Research Initiative (NRI) via Midwest Institute for Nanoelectronics Discovery (MIND) and by Kentucky Science Technology Corporation (#KSTC-184-512-10-081). We thank Tom Kopley, Ron Reifenberger, Leonid Rokhinson and Lishan Weng for helpful discussions and John Coy for technical assistance.

References

[1] Geim A K and Novoselov K S 2007 *Nat. Mater.* **6** 183
[2] Geim A K 2009 *Science* **324** 1530
[3] Novoselov K S, Geim A K, Morozov S V, Jiang D, Zhang Y, Dubonos S V, Grigorieva I V and Firsov A A 2004 *Science* **306** 666
[4] Wang X, Li X, Zhang L, Yoon Y, Weber P K, Wang H, Guo J and Dai H 2009 *Science* **324** 768
[5] Wehling T O, Novoselov K S, Morozov S V, Vdovin E E, Katsnelson M I, Geim A K and Lichtenstein A I 2008 *Nano Lett.* **8** 173
[6] Giovannetti G, Khomyakov P A, Brocks G, Karpan V M, van den Brink J and Kelly P J 2008 *Phys. Rev. Lett.* **101** 026803
[7] Adam S, Hwang E H, Galitski V M and Das Sarma S 2007 *Proc. Natl Acad. Sci. USA* **104** 18392
[8] Martin J, Akerman N, Ulbrich G, Lohmann T, Smet J H, Von Klitzing K and Yacoby A 2008 *Nature Phys.* **4** 145
[9] Kim E A and Castro Neto A N 2008 *Europhys. Lett.* **84** 57007
[10] Chen J H, Jang C, Adam S, Fuhrer M S, Williams E D and Ishigami M 2008 *Nature Phys.* **4** 377
[11] Zhang Y, Brar V W, Girit C, Zett A and Crommie M F 2009 *Nature Phys.* **5** 722
[12] Dan Y, Lu Y, Kybert N, Luo Z and Johnson A T 2009 *Nano Lett.* **9** 1472
[13] Golizadeh-Mojarad R and Datta S 2009 *Phys. Rev.* B **79** 085410
[14] Cho S and Fuhrer M S 2008 *Phys. Rev.* B **77** 081402
[15] Huard B, Stander N, Sulpizio J A and Goldhaber-Gordon D 2008 *Phys. Rev.* B **78** 121402
[16] Blake P, Wang R, Morozov S V, Schedin F, Ponomarenko L A, Zhukov A A, Nair R R, Grigorieva I V, Novoselov K S and Geim A K 2009 *Solid State Commun.* **149** 1068
[17] Deshpande A, Bao W, Miao F, Lau C N and LeRoy B J 2009 *Phys. Rev.* B **79** 205411
[18] Lee E J H, Balasubramanian K, Weitz R T, Burghard M and Kern K 2008 *Nat. Nanotechnol.* **3** 486
[19] Mueller T, Xia F, Freitag M, Tsang J and Avouris P 2009 *Phys. Rev.* B **79** 245430
[20] Xu X, Gabor N M, Alden J S, Van der Zande A M and McEuen P L 2010 *Nano Lett.* **10** 562
[21] Eriksson M A, Beck R G, Topinka M, Katine J A, Westervelt R M, Campman K L and Gossard A C 1996 *Appl. Phys. Lett.* **69** 671
[22] Eriksson M A, Beck R G, Topinka M, Katine J A, Westervelt R M, Campman K L and Gossard A C 1996 *Superlatt. Microstruct.* **20** 435
[23] Topinka M A, LeRoy B J, Westervelt R M, Shaw S E J, Fleischmann R, Heller E J, Maranowski K D and Gossard A C 2001 *Nature* **410** 183
[24] Aoki N, da Cunha C R, Akis R, Ferry D K and Ochiai Y 2005 *Phys. Rev.* B **72** 155327
[25] Yang C, Zhong Z and Lieber C M 2005 *Science* **310** 1304
[26] Bachtold A, Fuhrer M S, Plyasunov S, Forero M, Anderson E H, Zettl A and McEuen P L 2000 *Phys. Rev. Lett.* **84** 6082
[27] Tans S J and Dekker C 2000 *Nature* **404** 834
[28] Bockrath M, Liang W, Bozovic D, Hafner J H, Lieber C M, Tinkham M and Park H 2001 *Science* **29** 283
[29] Freitag M, Johnson A T, Kalinin S V and Bonnell D A 2002 *Phys. Rev. Lett.* **89** 216801
[30] Berezovsky J, Borunda M F, Heller E J and Westervelt R M 2010 *Nanotechnology* **21** 274013
Berezovsky J and Westervelt R M 2010 *Nanotechnology* **21** 274014
[31] Schnez S, Güttinger J, Huefner M, Stampfer C, Ensslin K and Ihn T 2010 *Phys. Rev.* B **82** 165445

[32] Connolly M R, Chiou K L, Smith C G, Anderson D, Jones G A C, Lombardo A, Fasoli A and Ferrari A C 2010 *Appl. Phys. Lett.* **96** 113501
[33] Connolly M R and Smith C G 2010 *Phil. Trans. R. Soc.* A **368** 5379
[34] Wilson R N and Cobden D H 2008 *Nano Lett.* **8** 2161
[35] Yazdanpanah M M, Harfenist S A, Safir A and Cohn R W 2005 *J. Appl. Phys.* **98** 073510
[36] Yazdanpanah M M 2006 Near room temperature self-assembly of nanostructure through gallium reaction with metal thin films *PhD Dissertation* University of Louisville
[37] Ferrari A C *et al* 2006 *Phys. Rev. Lett.* **97** 187401
[38] Novoselov K S, Geim A K, Morozov S V, Jiang D, Katsnelson M I, Grigorieva I V, Dubonos S V and Firsov A A 2005 *Nature* **438** 197
[39] Zhang Y, Tan Y W, Stormer H L and Kim P 2005 *Nature* **438** 201
[40] Castro Neto A H, Guinea F, Peres N M R, Novoselov K S and Geim A K 2009 *Rev. Mod. Phys.* **81** 109
[41] Rossi E and Das Sarma S 2008 *Phys. Rev. Lett.* **101** 166803
[42] Aoki N, Sudou K, Matsusaki K, Okamoto K and Ochiai Y 2008 *J. Phys.: Conf. Ser.* **109** 012007
[43] Schedin F, Geim A K, Morozov S V, Hill E W, Blake P, Katsnelson M I and Novoselov K S 2007 *Nat. Mater.* **6** 652
[44] Wilson N R and MacPherson J V 2009 *Nat. Nanotechnol.* **4** 483
[45] Morozov S V, Novoselov K S, Katsnelson M I, Schedin F, Ponomarenko L A, Jiang D and Geim A K 2006 *Phys. Rev. Lett.* **97** 016801
[46] Yu Y J, Zhao Y, Ryu S, Brus L E, Kim K S and Kim P 2009 *Nano Lett.* **9** 3430